Ultra-low-loss high-aspect-ratio Si_3N_4 waveguides

Jared F. Bauters,[1,*] Martijn J. R. Heck,[1] Demis John,[1] Daoxin Dai,[1] Ming-Chun Tien,[1] Jonathon S. Barton,[1] Arne Leinse,[2] René G. Heideman,[2] Daniel J. Blumenthal,[1] and John E. Bowers[1]

[1]*Department of Electrical and Computer Engineering, University of California, Santa Barbara, California 93106, USA*
[2]*LioniX BV, P.O. Box 456, 7500 AH, Enschede, Netherlands*
**jbauters@ece.ucsb.edu*

Abstract: We characterize an approach to make ultra-low-loss waveguides using stable and reproducible stoichiometric Si_3N_4 deposited with low-pressure chemical vapor deposition. Using a high-aspect-ratio core geometry, record low losses of 8-9 dB/m for a 0.5 mm bend radius down to 3 dB/m for a 2 mm bend radius are measured with ring resonator and optical frequency domain reflectometry techniques. From a waveguide loss model that agrees well with experimental results, we project that 0.1 dB/m total propagation loss is achievable at a 7 mm bend radius with this approach.

OCIS codes: (130.0130) Integrated optics; (230.7390) Waveguides, planar.

References and links

1. H. Takahashi, "Planar lightwave circuit devices for optical communication: present and future," Proc. SPIE **5246**, 520–531 (2003).
2. C. Ciminelli, F. Dell'Olio, C. E. Campanella, and M. N. Armenise, "Photonic technologies for angular velocity sensing," Adv. Opt Photon. **2**(3), 370–404 (2010).
3. E. F. Burmeister, J. P. Mack, H. N. Poulsen, M. L. Masanović, B. Stamenić, D. J. Blumenthal, and J. E. Bowers, "Photonic integrated circuit optical buffer for packet-switched networks," Opt. Express **17**(8), 6629–6635 (2009).
4. K. Horikawa, I. Ogawa, T. Kitoh, and H. Ogawa, "Silica-based integrated planar lightwave true-time-delay network for microwave antenna applications," in *Proceedings of the Optical Fiber Communication Conference*, (San Jose, Calif., 1996), Vol. 2, pp. 100–101.
5. Y. Li, and C. Henry, "Silica-based optical integrated circuits," IEE Proc., Optoelectron. **143**(5), 263 (1996).
6. B. Larsen, L. Nielsen, K. Zenth, L. Leick, C. Laurent-Lund, L. Andersen, and K. Mattsson, "A Low-Loss, Silicon-Oxynitride Process for Compact Optical Devices," in *Proceedings of ECOC* (Rimini, Italy, 2003).
7. R. Adar, M. Serbin, and V. Mizrahi, "Less than 1 dB per meter propagation loss of silica waveguides measured using a ring resonator," J. Lightwave Technol. **12**(8), 1369–1372 (1994).
8. T. Kominato, Y. Hida, M. Itoh, H. Takahashi, S. Sohma, T. Kitoh, and Y. Hibino, "Extremely low-loss (0.3 dB/m) and long silica-based waveguides with large width and clothoid curve connection," in *Proceedings of ECOC* (Stockholm, Sweden, 2004).
9. F. Morichetti, A. Melloni, M. Martinelli, R. G. Heideman, A. Leinse, D. H. Geuzebroek, and A. Borreman, "Box-Shaped Dielectric Waveguides: A New Concept in Integrated Optics?" J. Lightwave Technol. **25**(9), 2579–2589 (2007).
10. F. P. Payne, and J. P. Lacey, "A theoretical analysis of scattering loss from planar optical waveguides," Opt. Quantum. Electron. **26**(10), 977–986 (1994).
11. A. Melloni, F. Morichetti, R. Costa, G. Cusmai, R. Heideman, R. Mateman, D. Geuzebroek, and A. Borreman, "TriPleX^{TM}: a new concept in optical waveguiding," in *Proceedings of the 13th European Conference on Integrated Optics* (Copenhagen, Denmark, 2007), pp. 3–6.
12. D. Dai, J. F. Bauters, M. Tien, M. Heck, D. Blumenthal, and J. E. Bowers, "Polarization characteristics of low-loss nano-core buried optical waveguides and directional couplers," in *Proceedings of GFP* (Beijing, China, 2010).
13. F. Ay, and A. Aydinli, "Comparative investigation of hydrogen bonding in silicon based PECVD grown dielectrics for optical waveguides," Opt. Mater. **26**(1), 33–46 (2004).
14. S. Sakaguchi, S. Todoroki, and S. Shibata, "Rayleigh scattering in silica glasses," J. Am. Ceram. Soc. **79**(11), 2821–2824 (1996).
15. T. Barwicz, and H. Haus, "Three-dimensional analysis of scattering losses due to sidewall roughness in microphotonic waveguides," J. Lightwave Technol. **23**(9), 2719–2732 (2005).

#136596 - $15.00 USD Received 13 Oct 2010; revised 9 Dec 2010; accepted 13 Dec 2010; published 3 Feb 2011

16. C. Ciminelli, V. M. Passaro, F. Dell'Olio, and M. N. Armenise, "Three-dimensional modelling of scattering loss in InGaAsP/InP and silica-on-silicon bent waveguides," J. Eur. Opt. Soc. Rapid Publ. **4**, 1–6 (2009).
17. A. B. Fallahkhair, K. S. Li, and T. E. Murphy, "Vector Finite Difference Modesolver for Anisotropic Dielectric Waveguides," J. Lightwave Technol. **26**(11), 1423–1431 (2008).
18. K. K. Lee, D. R. Lim, H. Luan, A. Agarwal, J. Foresi, and L. C. Kimerling, "Effect of size and roughness on light transmission in a Si/SiO_2 waveguide: Experiments and model," Appl. Phys. Lett. **77**(11), 1617–1619 (2000).
19. M. Heiblum, and J. Harris, "Analysis of curved optical waveguides by conformal transformation," IEEE J. Quantum. Electron. **11**(2), 75–83 (1975).
20. P. Bienstman, E. Six, A. Roelens, M. Vanwolleghem, and R. Baets, "Calculation of bending losses in dielectric waveguides using eigenmode expansion and perfectly matched layers," IEEE Photon. Technol. Lett. **14**(2), 164–166 (2002).
21. T. Barwicz, and H. Smith, "Evolution of line-edge roughness during fabrication of high-index-contrast microphotonic devices," J. Vac. Sci. Technol. B **21**(6), 2892 (2003).
22. M. John, Senior, *Optical Fiber Communications Principles and Practice Second Edition* (Pearson Education, 1992).
23. G. Bona, R. Germann, F. Horst, B. Offrein, and H. Salemink, "Versatile silicon-oxynitride planar lightwave circuits for interconnect applications," in *Proceedings of the 6th International Conference on Parallel Interconnects* (1999), pp. 145–148.
24. M. Fadel, and E. Voges, "Low-Loss SiON Ring Resonators on Silicon for 1.55 μm Wavelength," in *Proceedings of the 13th European Conference on Integrated Optics* (Copenhagen, Denmark, 2007), WG3.
25. Y. Hibino, H. Okazaki, Y. Hida, and Y. Ohmori, "Propagation loss characteristics of long silica-based optical waveguides on 5 inch Si wafers," Electron. Lett. **29**(21), 1847–1848 (1992).
26. J. Guo, G. A. Vawter, M. J. Shaw, G. R. Hadley, P. Esherick, A. Jain, and C. R. Alford, "Characterization of Si_3N_4/SiO_2 planar lightwave circuits and ring resonators," in Proc. SPIE **5350**, 13–22 (2004).
27. A. Yeniay, R. Gao, K. Takayama, R. Gao, and A. Garito, "Ultra-Low-Loss Polymer Waveguides," J. Lightwave Technol. **22**(1), 154–158 (2004).
28. M. Y. T. Kominato, Y. Ohmori, H. Okazaki, and M. Yasu, "Very low-loss GeO_2-doped silica waveguides fabricated by flame hydrolysis deposition method," Electron. Lett. **26**(5), 327–329 (1990).
29. Y. Hida, Y. Hibino, H. Okazaki, and Y. Ohmori, "10 m long silica-based waveguide with a loss of 1.7 dB/m," in *Integrated Photonics Research*, Vol. 7 of 1995 OSA Technical Digest Series (Optical Society of America, 1995), paper IThC6.
30. R. A. Bellman, G. Bourdon, and G. Alibert, A. Beguin, E. Guiot, L. B. Simpson, P. Lehuede, L. Guiziou, and E. LeGuen, "Ultralow Loss High Delta Silica Germania Planar Waveguides," J. Electrochem. Soc. **151**, G541 (2004).
31. D. Klunder, E. Krioukov, F. Tan, T. Van Der Veen, H. Bulthuis, G. Sengo, C. Otto, H. Hoekstra, and A. Driessen, "Vertically and laterally waveguide-coupled cylindrical microresonators in Si_3N_4 on SiO_2 technology," Appl. Phys. B **73**, 603–608 (2001).
32. F. Horst, R. Beyeler, G. Bona, E. Flück, R. Germann, B. Offrein, H. Salemink, and D. Wiesmann, "Compact, tunable optical devices in silicon-oxynitride waveguide technology," in *Integrated Photonics Research*, T. Li, ed., Vol. 45 of OSA Trends in Optics and Photonics (Optical Society of America, 2000), paper IThF1.

1. Introduction

Compared to bulk and fiber optic systems, photonic integrated circuits (PICs) can offer improved performance and stability in a smaller footprint and at a lower cost. Many targeted PIC applications, for example, communication network filters and multiplexers [1], optical gyroscope rotational velocity sensors [2], optical buffers [3], and true-time-delay antenna beam-steering networks [4], require large on-chip optical path lengths and/or high-quality-factor resonators. As performance demands on these applications increase, waveguides with ultra-low propagation loss become necessary.

With propagation losses less than 1 dB/cm at $\lambda = 1550$ nm for bend radii down to 0.5 mm, silica-on-silicon planar lightwave circuits (PLCs) have been most successful in meeting this challenge. In a PLC, ultra-low loss is commonly achieved with a low-index-contrast core buried between 10 to 20 microns of silicon dioxide [5]. The core is typically square or nearly-square with side lengths of several microns in order to maintain low polarization sensitivity, efficient fiber coupling, and single-mode operation for passive communication network applications. Several core materials and deposition processes with varying index contrasts have been pursued within this general framework. Propagation loss as low as 5 dB/m at a 2 mm bend radius has been reported for silicon oxynitride cores having an index contrast of 2.5% [6]. Phosphorus-doped SiO_2 cores with an index contrast of 0.6-0.7% have reached losses of 0.85, 1.22, and 4.72 dB/m at 30, 20, and 10 mm bend radii, respectively [7]. In [8], germanium-doped SiO_2 waveguides deposited with flame hydrolysis at an index contrast of

#136596 - $15.00 USD Received 13 Oct 2010; revised 9 Dec 2010; accepted 13 Dec 2010; published 3 Feb 2011

0.75% show an average propagation loss of 0.3 dB/m. In this case, however, the large core dimensions result in a "quasi-single-mode" waveguide, meaning that higher-order modes can be excited but are lost while propagating through waveguide bends.

Stoichiometric silicon nitride has a higher refractive index contrast with SiO_2 than the above core materials and offers the benefits of increased material stability and high refractive index regularity. Moreover, Si_3N_4 films deposited with low-pressure chemical vapor deposition (LPCVD) have thicknesses controllable to the nanometer scale and exhibit low (< 0.4 nm) surface roughness, a quality necessary for maintaining low scattering loss at the top and bottom core-cladding interfaces [9]. Since interfacial scattering loss scales quadratically with the difference between the core and cladding permittivities [10], the high refractive index contrast (around 25%) of stoichiometric Si_3N_4 with SiO_2 could potentially prevent the realization of ultra-low-loss waveguides made from this material. Sidewall scattering, the primary contributor to loss in high-index-contrast planar waveguides, can be minimized, however, by using a high-aspect-ratio core geometry in which the width of the waveguide far exceeds the thickness. This allows one to keep the benefits of a stoichiometric material while also attaining low propagation loss.

In this paper, we report on single-mode ultra-low-loss waveguides (ULLWs) fabricated with TriPleX^{TM} LPCVD Si_3N_4 technology [11] for a design wavelength of 1550 nm. As the core refractive index is fixed, a design-by-geometry approach allows ultra-low loss to be achieved across a range of millimeter-scale bend radii using the high-aspect-ratio (width:thickness > 10:1) and low-confinement core design shown to scale in Fig. 1. As reported in [12], the confinement of the fundamental TM mode, Γ_{xy}^{TM}, is much lower than that of the fundamental TE mode, Γ_{xy}^{TM}, in such high-aspect-ratio designs, and the high birefringence increases the polarization maintaining properties of the waveguide. For the 80 nm-thick waveguide shown in Fig. 1, $\Gamma_{xy}^{TE} / \Gamma_{xy}^{TM} \cong 7.6$, so that only the propagation loss and design for the fundamental TE mode are considered. We begin with an outline of the waveguide loss model used in the design of the waveguides (Section 2). We then discuss the characterization of ultra-low waveguide loss using ring resonator and optical frequency domain reflectometry (OFDR) measurements (Section 3). Finally, we use the characterization results along with our model to project how stoichiometric Si_3N_4 waveguides with propagation loss on the order of 0.1 dB/m can be realized (Section 4).

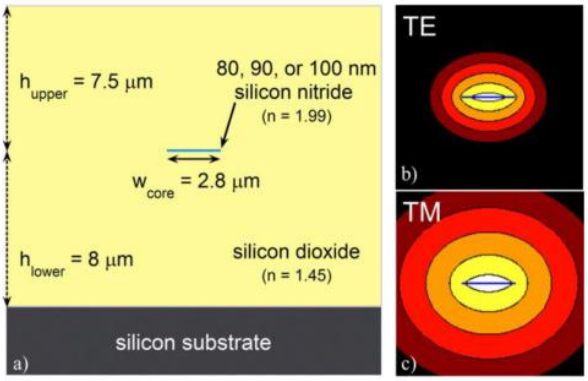

Fig. 1. (a) Cross-section (to scale) of the Si_3N_4-core waveguides designed and characterized in this paper along with simulated (λ = 1550 nm) fundamental (b) TE and (c) TM modes (same scale) of an 80 nm core waveguide. The spacing between contours is 6 dB down to the minimum contour of −30 dB.

#136596 - $15.00 USD Received 13 Oct 2010; revised 9 Dec 2010; accepted 13 Dec 2010; published 3 Feb 2011

2. Loss model

In a planar waveguide, the total propagation loss of a mode is the sum of many contributions including material absorption, Rayleigh scattering, interfacial scattering, substrate leakage, bend radiation, and crosstalk loss. At the cost of increased fabrication time, substrate leakage can be rendered negligible (~0.001 dB/m for the layers shown in Fig. 1(a)) through the deposition of thick cladding layers. Similarly, crosstalk loss can also be neglected if sufficient space is included between waveguide cores. Material absorption loss in a PLC is primarily due to absorptive bond resonances, typically involving hydrogen, present within the core and cladding layers. In [13], a high temperature (1000 °C) anneal is shown to decrease the concentration of loss-dominating N-H bonds in SiON material to a level well below the detection limit of common measurement techniques or less than 0.5x1021 cm−3. An extrapolation from the available data taken at λ = 1530 nm in [13] suggests that N-H bond concentrations on the order of 1x1020, 1x1019, and 1x1018 cm−3 would contribute ~1, 0.1, and 0.01 dB/m to the total propagation loss in a low-confinement Si3N4 waveguide with $\Gamma_{xy} \cong 0.1$. Since the waveguides considered in this paper are low-confinement and annealed for several hours above 1100 °C, material loss is not included in the model. Rayleigh scattering, accounting for a propagation loss on the order of 0.1 dB/km, is also negligible compared to interfacial scattering and bend radiation loss in planar dielectric waveguides [14]. Since an additional loss contribution can arise from scattering and bend-induced conversion to higher order modes in a multimode waveguide, core geometries should support a single guided mode at λ = 1550 nm. Thus, a model that considers scattering loss at all core-cladding interfaces, bend radiation loss, and single-mode core geometries is employed.

2.1 Interface scattering loss model

In order to include the full effect of the core geometry, we use a three-dimensional volume current method to calculate interfacial scattering loss [15,16]. In this approach, the interface roughness profile, f(z) in Fig. 2(a), gives the deviation of the core-cladding interface from its mean location, which is taken to be zero. The deviation is assumed to be a function of the propagation direction alone, yielding a columnar description of the interface roughness. The radiation loss due to scattering from the refractive index inhomogeneity at this rough interface is then modeled as an equivalent polarization volume current density. This equivalent source is proportional to the electric field at the core-cladding interface of the waveguide. As the mean deviation in the interface location is typically a small fraction of the waveguide cross-section, the mode of the unperturbed waveguide can be used as an accurate approximation of the field distribution in the rough waveguide. For example, at the sidewall interface shown in Fig. 2 and for the waveguide's fundamental TE mode [15]:

$$\vec{J}(\vec{r}) = -j\omega\varepsilon_0\left(n_{core}^2 - n_{clad}^2\right)\vec{E}_{TE}(x,y)\delta(y)\delta(z), \qquad (1)$$

where $-\frac{a}{2} \le x \le \frac{a}{2}$, ω is the radial frequency of the light propagating in the waveguide, ε_0 is the permittivity of free space, $\left(n_{core}^2 - n_{clad}^2\right)$ is the difference of the core and cladding relative dielectric constants, $\vec{E}_{TE}(x,y)$ is the electric field of the fundamental TE mode of the waveguide, and $\delta(y)$ is the Dirac delta function. The x, y, and z components of the electric field at each core-cladding interface are calculated numerically with a fully vectorial finite-difference algorithm incorporated into MATLAB [17].

#136596 - $15.00 USD Received 13 Oct 2010; revised 9 Dec 2010; accepted 13 Dec 2010; published 3 Feb 2011

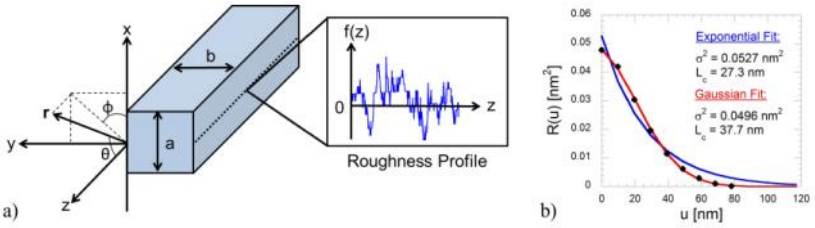

Fig. 2. (a) Coordinate system referenced in all equations along with waveguide roughness profile and (b) autocorrelation function of AFM data from the surface of a Si_3N_4 film fit to exponential and Gaussian models.

As shown in Fig. 2(b), we assume that the autocorrelation function of the roughness profile, $R(u) = \langle f(z) f(z+u) \rangle$, measured at the core-cladding interface of a waveguide fits well to an exponential model [10,15,16]:

$$R(u) \approx \sigma^2 \exp\left(-\frac{|u|}{L_c}\right), \tag{2}$$

where σ^2, the mean square deviation, and L_c, the correlation length of the roughness, are the model fitting parameters. Furthermore, the power spectrum of the roughness, $\tilde{R}(\Omega)$, is related to the autocorrelation function by a Fourier transform [15]:

$$\tilde{R}(\Omega) = \Im\{R(u)\} \approx \frac{2\sigma^2 L_c}{1+L_c^2\Omega^2}. \tag{3}$$

The power spectrum is the intensity with which a spatial frequency Ω is present in the interface roughness profile. As such, the product of the power spectrum with the power radiation pattern of the current source in Eq. (1) forms the final power radiation pattern of the interface scattering's equivalent current source, and the total power per unit length radiated by this source is calculated as:

$$\frac{P_{rad}}{L} = \int_0^{2\pi}\int_0^{\pi} \left(\vec{S}\cdot\hat{r}\right)\tilde{R}\left(\beta - k_0 n_{clad}\hat{r}\cdot\hat{z}\right) r^2 \sin\theta d\theta d\phi, \tag{4}$$

where $\left(\vec{S}\cdot\hat{r}\right)$ is the outward directed Poynting vector due to the current source in Eq. (1), β is the propagation constant of the mode, and k_0 is the free space wavenumber. The integration of $\tilde{R}(\Omega)$ is limited to spatial frequencies between $\left(\beta - k_0 n_{clad}\hat{r}\cdot\hat{z}\right)$ and $\left(\beta + k_0 n_{clad}\hat{r}\cdot\hat{z}\right)$, as this interval is responsible for the roughness-induced coupling to radiation modes [10]. In order to calculate the power loss coefficient α due to the radiation from the interface, P_{rad}/L is divided by the total z-directed Poynting vector in the waveguide mode. If the roughness profiles at each core-cladding interface are uncorrelated, Eq. (4) can be applied independently at each rough surface in order to calculate the total scattering loss.

For low index contrast waveguides, the power radiated from the equivalent current source is calculated to good approximation by assuming that the current source radiates into a uniform medium with refractive index equal to that of the cladding. Under this assumption, $\left(\vec{S}\cdot\hat{r}\right)$ can be calculated using the magnetic vector potential in the Lorenz gauge [15,16]. Since Si_3N_4 has a relatively high index contrast of ~25% with SiO_2, the waveguide core's effect on the power radiation profile of the equivalent current source must be considered. This is accomplished analytically using the dyadic Green's functions of one-layer media presented in [15]. The final expression for $\left(\vec{S}\cdot\hat{r}\right)$, valid for any index contrast is then:

#136596 - $15.00 USD Received 13 Oct 2010; revised 9 Dec 2010; accepted 13 Dec 2010; published 3 Feb 2011

$$\left(\vec{S}\cdot\hat{r}\right)=\frac{\pi^2 n_{clad}}{2\lambda_0^4\eta_0 r^2}\left(n_{core}^2-n_{clad}^2\right)^2\,\mathrm{Re}\left\{\bar{\bar{G}}\bar{\bar{G}}^*\right\}\left|F_{shape}(\theta,\phi)\right|^2\left|S_{pol}(\theta,\phi)\right|^2, \qquad (5)$$

where η_0 is the impedance of free space, λ_0 is the free space wavelength, $\bar{\bar{G}}$ is the dyadic Green's function for one-layer media, $\left|F_{shape}(\theta,\phi)\right|^2$ is the power array factor corresponding to the electric field shape at the sidewall as defined in [15], and $\left|S_{pol}(\theta,\phi)\right|^2$ is the normalized power radiation profile of a point source with x, y, or z polarization, e.g. $\left|S_{pol}(\theta,\phi)\right|^2=\sin^2(\theta)$ for x polarization. Since we have extended the scattering loss model in [15] to include scattering from the top and bottom core-cladding interfaces, an additional field shape, $\Upsilon_z(y)$, is used to better match the z component of $\vec{E}_{TE}(x,y)$ there:

$$\Upsilon_z(y)=\sqrt{\tfrac{2}{b}}\left|\sin\left(\tfrac{\pi y}{b}\right)\right|, \qquad (6)$$

$$\left|F_{|\sin|}(\theta,\phi)\right|^2=\frac{8b\left[\pi-bn_{clad}k_0\cos(\phi)\sin(\theta)\sin\left(\frac{1}{2}bn_{clad}k_0\cos(\phi)\sin(\theta)\right)\right]^2}{\left(\pi-bn_{clad}k_0\cos(\phi)\sin(\theta)\right)^2\left(\pi+bn_{clad}k_0\cos(\phi)\sin(\theta)\right)^2}, \qquad (7)$$

where b is the waveguide core width as shown in Fig. 2. In [18], the TE propagation loss in a 200 x 500 nm silicon nanowire (n_{core} - n_{clad} = 2.0) is measured to be ~33 dB/cm at λ_0 = 1540 nm. Using the measured σ and L_c of 9 and 50 nm, the model predicts a scattering loss of 33.41 dB/cm, giving a ~1% error.

2.2 Bend radiation loss model

To simulate bend radiation loss, the curved waveguide is transformed into an equivalent straight waveguide through a conformal mapping of the refractive index [19]. A "staircase" consisting of 200 uniform layers approximates the resultant non-uniform refractive index profile, and an eigenmode expansion method (CAMFR [20]) is used to solve for the modes of this structure. With a non-uniform refractive index profile, the mode solution becomes radiative wherever the refractive index is greater than the modal index. By adding perfectly matched layers (PML) at the boundaries of the simulation window, this radiation loss is quantified in the imaginary part of the modal index [20]. From such a model, it is intuitive that higher confinement structures with larger modal indices result in lower bend loss for a given bend radius.

2.3 Waveguide design from loss model

We now consider the design of Si_3N_4-core strip waveguides as shown in Fig. 1. Scattering loss due to the sidewall, top, and bottom interfaces is plotted for different core geometries in Fig. 3. The roughness parameters at opposite sidewalls and at the top and bottom interfaces are assumed to be equal, and only results from core geometries operating in the single-mode regime are shown. Typical sidewall roughness correlation lengths resulting from planar waveguide fabrication processes range from 20 to 70 nm [21], and scattering loss at λ_0 = 1550 nm depends linearly on L_c in this regime. To be consistent with previous scattering loss analyses [15,16], a value of L_c = 50 nm is assumed for all plots with simulated sidewall scattering loss. From our own atomic force microscope (AFM) measurements of Si_3N_4 films (Fig. 2(b)), typical top surface roughness correlation lengths are closer to 30 nm, and this value is assumed for all plots with simulated top and bottom surface scattering loss. As Eq. (3) contains the only dependence of scattering loss on mean square deviation, loss can be calculated from Fig. 3 in units of dB/m through multiplication by the σ^2 that is characteristic of that interface:

#136596 - $15.00 USD Received 13 Oct 2010; revised 9 Dec 2010; accepted 13 Dec 2010; published 3 Feb 2011

$$\alpha_{total} = \sigma^2_{sidewall}\Pi_{sidewall} + \sigma^2_{top/bottom}\Pi_{top/bottom} \quad (8)$$

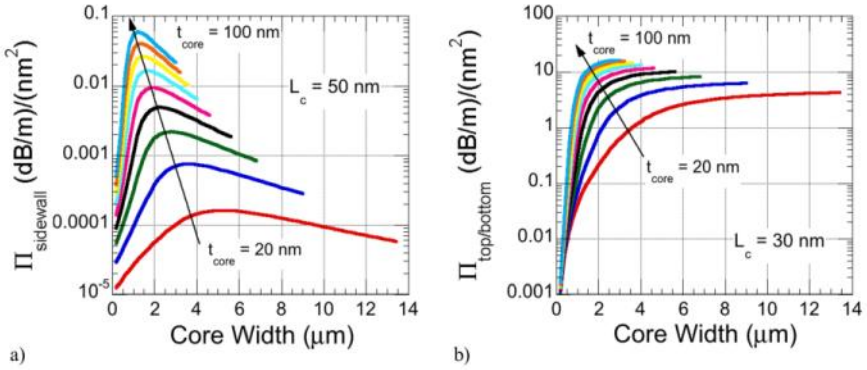

Fig. 3. Simulated (λ = 1550 nm) a) sidewall and b) top/bottom surface scattering losses for the fundamental TE mode of Si_3N_4 core waveguides. Loss is obtained through multiplication by the mean square deviation, σ^2, of the roughness profile.

The interfacial scattering loss curves in Fig. 3 are most easily understood within the context of Eq. (1) and the relationship between mode size, mode confinement, and core geometry presented in Fig. 4. In Fig. 3(a) and Fig. 4(a), it can be seen that sidewall scattering loss increases with increasing core width at first as the mode transitions from being "squeezed out" to being more confined in the lateral direction. Sidewall scattering loss then reaches its peak magnitude where the lateral mode diameter is small, and the integral of $\vec{E}_{TE}(x,y)$ along the sidewall has its greatest magnitude. After the peak in sidewall scattering loss and the minimum in mode diameter have been reached, Fig. 4 shows that the mode is highly confined to the waveguide core along the lateral dimension. A further increase of the core width then decreases the optical intensity (W/m^2) in the core, yielding a corresponding decrease in scattering loss according to Eq. (1). Contrary to the sidewall case, loss from the top and bottom surfaces increases monotonically with core thickness (Fig. 3(b)), as the Si_3N_4 core thicknesses considered are not large enough to achieve high mode confinement along the vertical dimension (Fig. 4(b)). Scattering from the top and bottom interfaces also increases monotonically with core width as the equivalent radiating current source described by Eq. (1) becomes larger.

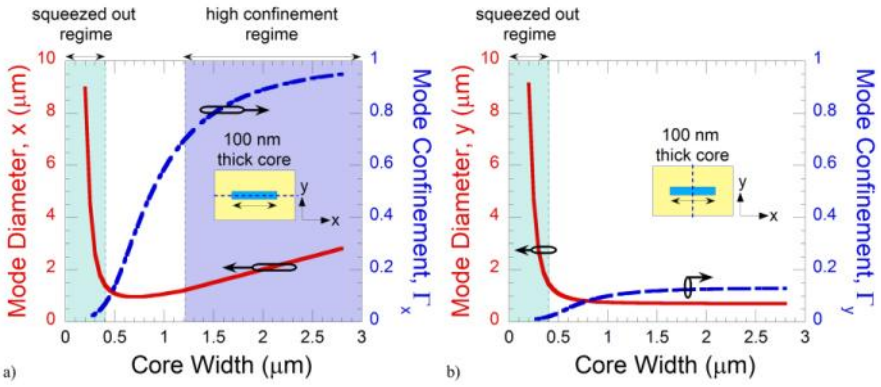

Fig. 4. Simulated (λ = 1550 nm) TE mode diameter (FWHM) and TE mode confinement along the a) lateral and b) vertical directions for varying waveguide core widths. The waveguide core thickness is 100 nm for both plots.

Though the lowest scattering loss is achieved in the squeezed out mode regime of Fig. 4, the low confinement of such a waveguide limits its application to very large bend radii or

#136596 - $15.00 USD Received 13 Oct 2010; revised 9 Dec 2010; accepted 13 Dec 2010; published 3 Feb 2011

efficient fiber-coupling spot-size-converters. Since a waveguide bend is a necessary component of any PIC, a trade-off between low scattering and a practical bend radius must be made. From Fig. 3 and Fig. 4, it can be seen that increasing the core width increases mode confinement and scattering loss from the top and bottom interfaces while also decreasing scattering loss from the sidewall interfaces. For planar waveguides, the $\sigma^2_{sidewall}$ due to an optimized dry etching of the core is typically around 10 nm^2 [15] while the $\sigma^2_{top/bottom}$ resulting from a polished deposited material is less than 0.1 nm^2. Therefore, decreasing $\Pi_{sidewall}$ at the cost of an increase in $\Pi_{top/bottom}$ will yield a decrease in total scattering loss up until sidewall scattering loss no longer dominates, that is, until $\Pi_{top/bottom}$ is greater than $\Pi_{sidewall}$ by about three orders of magnitude. This implies that the lowest loss Si_3N_4 core geometry for a given bend radius has the highest single-mode aspect ratio that can maintain low loss around a bend.

For the Si_3N_4-core waveguide fabrication run characterized in the next section of this paper, a minimum bend radius of 2 mm was chosen in order to fit the desired number of devices onto a single wafer. The run consisted of three core thicknesses. From our bend loss model, we determined that an 80 nm thick waveguide should not be bend loss limited at a bend radius of 2 mm. Therefore 80, 90, and 100 nm core thicknesses were targeted. To ensure single-mode operation in the 100 nm thick waveguides, a maximum waveguide width of 2.8 μm was used on the mask.

3. Waveguide loss characterization

Waveguide loss is often measured using cut-back and Fabry-Pérot resonator (Hakki-Paoli) techniques. For propagation losses on the order of 1 dB/m, cut-back structures must be multiple meters in length to allow for several detectable reductions in propagation loss. For a cut-back waveguide length difference of 1 m, the difference in output power is then also on the order of 1 dB, a value that does not far exceed the typical measurement error, e.g. due to a variance in coupling losses. Thus, long waveguide lengths or a large number of waveguide measurements are necessary to achieve sufficient accuracy . Likewise, the dependence of Fabry-Pérot resonator measurements on the waveguide facet power reflection coefficient can yield a measurement uncertainty on the same order as the total propagation loss in ultra-low-loss waveguides (a few dB). The measurement accuracy can be improved through careful facet preparation or by increasing the sample size of measured data, but both increase the measurement turnaround time. This is a particularly costly outcome if measurement results are to be used as part of a process or design optimization cycle where frequent and immediate feedback is desired.

3.1 Ring resonator measurements

As demonstrated in [7], ring resonators are suitable for measuring ultra-low propagation losses less than 1 dB/m. They also yield propagation loss for a fixed bend radius, clearly showing the bending capabilities of a given waveguide structure. Since the waveguide facets are not part of the resonator being characterized, the measurement is independent of the facet power reflection coefficient and fiber-waveguide coupling loss, avoiding the abovementioned difficulties. In this technique, the output power transmission spectrum of a ring resonator is fit to an (N+1) parameter model where N is the number of waveguides coupled to the ring. If a single waveguide with input and output ports is used, as is the case in this paper, the fit parameters are the round-trip loss of the resonator, γ_0, and the power coupling ratio of the straight-to-bent waveguide coupler, κ:

$$\frac{P_{out}}{P_{in}} = \left| \frac{\frac{\gamma_0 - \kappa}{2T} + j(\omega - \omega_0)}{\frac{\gamma_0 + \kappa}{2T} + j(\omega - \omega_0)} \right|^2, \tag{9}$$

where ω_0 is the resonant radial frequency and T is the round-trip time of the cavity. In order to obtain spectra with clear drops in output power at the resonant frequency, the resonators

#136596 - $15.00 USD Received 13 Oct 2010; revised 9 Dec 2010; accepted 13 Dec 2010; published 3 Feb 2011

should be designed such that γ_0 and κ are on the same order. Since κ depends primarily on the coupling gap, w_{gap}, between the straight waveguide and ring, it is controlled lithographically. As $d\kappa/dw_{gap}$ decreases exponentially with increasing w_{gap}, a larger w_{gap} increases the fabrication tolerance for the measurement structures. For the ring resonator measurement results shown in Fig. 5, a κ of ~0.01 was targeted with a w_{gap} ~2 μm. By measuring similar ring resonators (same γ_0) with varying κ, the measurement accuracy is further improved.

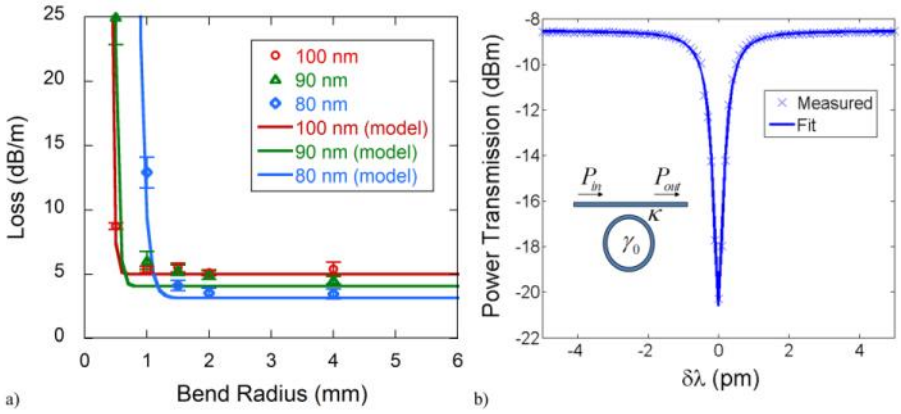

Fig. 5. (a) Ring resonator loss measurement results for 80, 90, and 100 nm waveguides at λ = ~1550 nm. Results are fit to the bend and scattering loss models (solid lines) using roughness parameters ($\sigma_{sidewall}$, L_c) = (14 nm, 50 nm) and ($\sigma_{surface}$, L_c) = (0.1 nm, 30 nm). (b) A typical measured output spectrum for a 100 nm thick, 4 mm radius ring.

In this work, ring resonators with 0.5, 1, 1.5, 2, and 4 mm radii are characterized. The spectra are obtained from the power transmission of the TE mode excited by a wavelength tunable laser with 100 kHz linewidth. By introducing this frequency resolution into the model given in Eq. (9), we confirm that a propagation loss on the order of 0.1 dB/m can be measured before the frequency granularity introduces a fit value error within an order of magnitude of the loss. Each ring has a single two-port coupling waveguide, and three power coupling ratios are achieved by curving this waveguide around the ring in order to change the length of the coupling region. The loss results from ring resonator measurements are shown in Fig. 5 along with a fit to these results using the loss model fitting parameters, $\sigma_{sidewall}$ and $\sigma_{surface}$. For the fit, typical sidewall and surface roughness correlation lengths are assumed. The fit yields roughness parameters ($\sigma_{sidewall}$, L_c) = (14 nm, 50 nm) and ($\sigma_{surface}$, L_c) = (0.1 nm, 30 nm). At a bend radius of 2 mm, the loss of each core thickness has reached its minimum, indicating that bend radiation loss is negligible for a bend radius greater than or equal to 2 mm as predicted by the bend loss model.

3.2 Reflectometry measurements

With optical reflectometry, one can measure the magnitude of the optical power backscattered from a propagation distance, W_0, within a waveguide. Assuming a uniform waveguide that is invariant in the propagation direction, the amount of power backscattered from W_0 is directly proportional to the amount of power present at W_0, and the return loss amplitude is given by [22]:

$$RL(z) = 10\log\left[\frac{P_{backscattered}(z)}{P_{in}}\right] = 10\log\left[S\alpha_R W_0 \exp(-2\alpha z)\right], \qquad (10)$$

where S is the fraction of reflected power captured by the waveguide, α_R is the backscatter loss coefficient, W_o is the spatial resolution of the reflectometry instrument, and α is the power attenuation coefficient of the propagating mode. The propagation loss of the waveguide can then be calculated by taking half of the slope in return loss with respect to distance. As

#136596 - $15.00 USD Received 13 Oct 2010; revised 9 Dec 2010; accepted 13 Dec 2010; published 3 Feb 2011

with ring resonators, the accuracy of a reflectometry measurement is independent of any variance in coupling loss or facet reflectivity. In Fig. 6, the large spikes in measured return loss amplitude demonstrate how reflectometry "sees" large scattering points in the optical path, allowing for the quantification of loss due to point defects separate from the distributed waveguide propagation losses.

In order to verify the ring resonator results, optical frequency domain reflectometry (Luna OBR 4400) is used to measure the propagation loss in 6 meters of spiraled waveguide. The spirals have a minimum bend radius of 2 mm at the S-bend in the center, so the bend loss is expected to be negligible for all waveguide thicknesses. The measured loss should then agree with the minimum loss measured with ring resonators at each thickness. Figure 6 shows the return loss amplitude versus length for an 80 nm thick waveguide spiral. The large spikes in return loss amplitude occur at the fiber-connector and fiber-waveguide interfaces. Index matching gel is used to reduce the reflection at the waveguide's input facet, and a polarization controller is employed in order to excite primarily the TE mode of the waveguide.

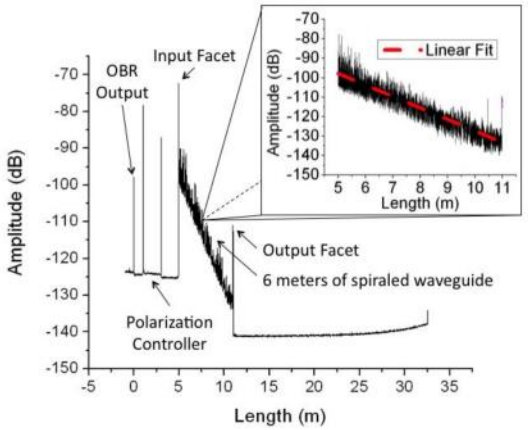

Fig. 6. Optical frequency domain reflectometry measurement of 6 meters of spiraled waveguide. The inset shows a linear fit to the decreasing return loss amplitude data that is used to extract propagation loss.

In OFDR, time domain return loss data is extracted from frequency domain data via a Fourier transform, and the spatial domain is then obtained using the group index of the propagating mode. The group velocity can be extracted by dividing the designed waveguide length by the measured delay between the input and output reflections in Fig. 6. This method yields group indices of 1.54, 1.57, and 1.59 for 80, 90, and 100 nm core thicknesses, respectively. These agree well with the group indices of 1.53, 1.55, and 1.57 simulated with PhotonDesign's FIMMWAVE software. In agreement with the ring resonator findings, linear fits of the OFDR return loss measurements give propagation losses of 2.91 +/– 0.01, 4.22 +/– 0.01, and 5.33 +/– 0.01 dB/m for the 80, 90, and 100 nm thick waveguides.

4. Comparison with state-of-the-art

Figure 7 shows the result of a thorough literature search for state-of-the-art propagation loss reported at a given bend radius in planar single-mode waveguides. Propagation loss values for silicon oxynitride, silicon nitride, Ge-doped SiO_2, P-doped SiO_2, and polymer waveguide cores are shown as red squares in the figure with index contrasts ranging from 0.25 to 25% [1,6,7,11,22–32]. For completeness, points are included for a typical silicon-on-insulator rib waveguide fabricated at UCSB, as well as the quasi-single-mode NTT result [8]. The Si_3N_4 core results reported in this paper are marked with blue triangles. To the best of our knowledge, the observed propagation loss of 8-9 dB/m at a 0.5 mm bend radius and for a 100 nm core thickness is ~90 dB/m lower than the previous lowest value reported for waveguides at that radius [11]. The 3 dB/m propagation loss measured at a 2 mm bend radius for an 80 nm

#136596 - $15.00 USD Received 13 Oct 2010; revised 9 Dec 2010; accepted 13 Dec 2010; published 3 Feb 2011

core thickness is 2 dB/m lower than the previous lowest value obtained with lower index contrast waveguides [1,6]. Furthermore, the results reported here fall on the leading edge of a loss-versus-radius boundary along which loss increases with decreasing bend radius. As one pursues smaller bend radii, tighter mode confinement is required, and larger core dimensions or higher refractive index contrasts are employed. This in turn increases the scattering loss of the waveguide assuming no improvement upon the typical roughness parameters obtainable with current fabrication technology.

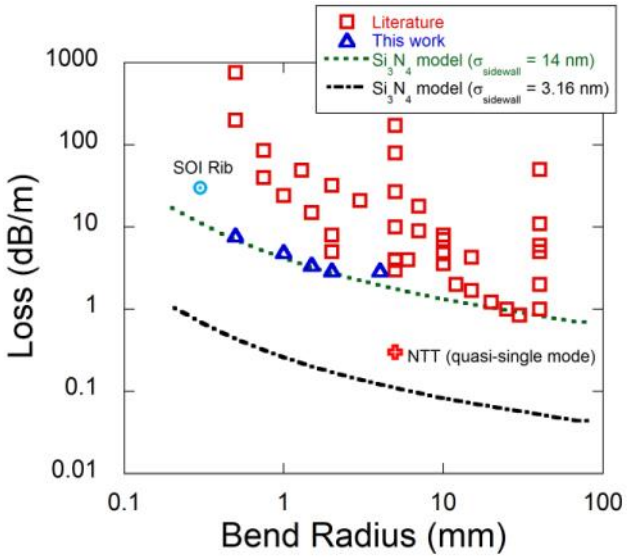

Fig. 7. A comparison of the high-aspect-ratio Si_3N_4-core loss results (blue triangles) with the state-of-the-art (red squares) [1,6,7,11,22–32]. Dashed lines show the minimum achievable loss at a given bend radius for Si_3N_4-core waveguides from the loss model using current ($\sigma_{sidewall}$ = 14 nm) and state-of-the-art ($\sigma_{sidewall}$ = 3.16 nm) roughness parameters.

The dashed lines in Fig. 7 show simulation results obtained from our loss model for Si_3N_4-core waveguides. The green (higher loss) curve shows the minimum achievable loss at a given bend radius using the already achieved roughness parameters of ($\sigma_{sidewall}$, L_c) = (14 nm, 50 nm) and ($\sigma_{surface}$, L_c) = (0.1 nm, 30 nm). The good fit of this line with measured waveguide loss suggests the valid exclusion of material absorption loss in our model for that regime. With a loss of ~17 dB/m at 0.2 mm down to ~1 dB/m at 10 mm, the loss model predicts record low loss for single-mode waveguides using the stoichiometric Si_3N_4 technology across the 0.2 – 10 mm bend radius regime. The black (lower loss) line shows the minimum achievable loss at a given bend radius if the mean deviation of the sidewall, $\sigma_{sidewall}$, is reduced to 3.16 nm. This value is reported in [15] as typical for an optimized etch process performed in a state-of-the-art fabrication facility. Additional loss measurements of lower confinement waveguides are necessary to confirm the valid exclusion of material absorption loss in our model for this regime.

Each point on the simulated loss vs. bend radius curves corresponds to the lowest-loss core geometry at that bend radius. Figure 8 shows how the lowest-loss core thickness and width change with increasing bend radius. As larger bend radii are used, lower confinement and higher-aspect-ratio waveguide cores yield the lowest achievable loss. From Fig. 7 and Fig. 8, propagation loss on the order of 0.1 dB/m can be achieved with stoichiometric LPCVD Si_3N_4 by increasing the aspect ratio of the waveguide core, using a larger minimum bend radius of 7 mm, and decreasing $\sigma_{sidewall}$ to ~3.1 nm through further optimization of the lithography and sidewall etch processes.

#136596 - $15.00 USD Received 13 Oct 2010; revised 9 Dec 2010; accepted 13 Dec 2010; published 3 Feb 2011

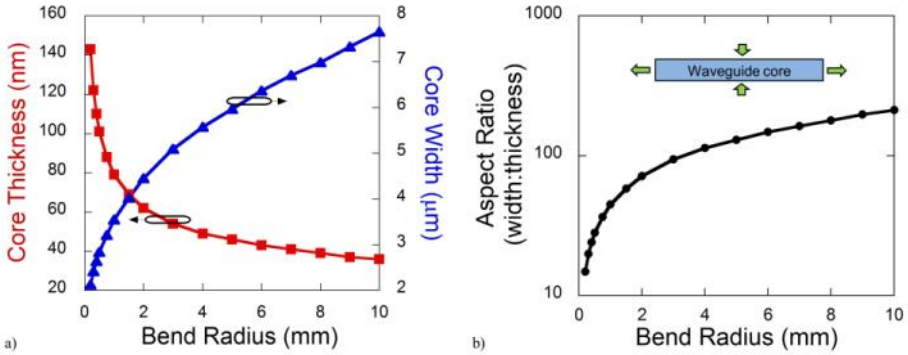

Fig. 8. (a) Simulated (λ = 1550 nm) lowest-loss single-mode core geometry and (b) aspect ratio are plotted versus bend radius.

5. Conclusions

An ultra-low-loss planar waveguide technology is demonstrated to bring the performance advantages of optical fiber-based devices to the chip scale. Although several low-index-contrast (Δn = 0.5 – 2.5%) technologies are also good ultra-low loss candidates, stoichiometric LPCVD Si_3N_4, with an index contrast of ~25%, offers the additional benefits of increased material uniformity and stability. Using a high-aspect-ratio core geometry, ultra-low loss can be obtained in single-mode Si_3N_4 waveguides at bend radii as low as 0.2 mm. In this work, we demonstrate record low losses of 8-9, 5, 3.5, and 3 dB/m at 0.5, 1, 1.5, and 2 mm bend radii, respectively. The challenge of measuring ultra-low loss with sufficient accuracy at chip-scale propagation lengths is met using ring resonator and OFDR techniques.

Acknowledgements

The authors thank Scott Rodgers and Wenzao Li for helpful discussions. This work is supported by DARPA MTO under iPhoD contract No: HR0011-09-C-0123.

#136596 - $15.00 USD Received 13 Oct 2010; revised 9 Dec 2010; accepted 13 Dec 2010; published 3 Feb 2011